Received: 25 November 2020 | Revised: 21 January 2021 | Accepted: 22 January 2021

DOI: 10.1002/app.50557

ARTICLE

Applied Polymer SCIENCE WILEY

Polypropylene/poly(ethylene terephthalate) microfibrillar reinforced composites manufactured by fused filament fabrication

Miaozi Huang[1] | **Alois K. Schlarb**[1,2,3]

[1]Chair of Composite Engineering (CCe), Technische Universität Kaiserslautern (TUK), Kaiserslautern, Germany

[2]Research Center OPTIMAS, Technische Universität Kaiserslautern (TUK), Kaiserslautern, Germany

[3]Qingdao University of Science and Technology, Qingdao, China

Correspondence
Alois K. Schlarb, Chair of Composite Engineering (CCe), Technische Universität Kaiserslautern (TUK), Gottlieb-Daimler-Str. Bld. 44, 67663 Kaiserslautern, Germany.
Email: alois.schlarb@mv.uni-kl.de

Abstract

In the present work, microfibrillar composites (MFCs) consisting of polypropylene (PP) and poly(ethylene terephthalate) (PET) were successfully produced by melt extrusion and cold stretching. The resulting filaments were then printed using fused filament fabrication. The morphological results demonstrate that the highly oriented PET fibrils after stretching are still well preserved in the printed components. Since the printing process defines the alignment of the fibrils in the final component the fibers can be perfectly adapted to the load paths. Comparative analyses of the mechanical properties reveal that the PET fibrils act as an effective reinforcement in the 3D printed components, resulting in the superior mechanical performance of the PP/PET MFCs compared to a PP/PET blend and a neat PP. Due to the combination of material and innovative processing, the study opens up a new way of using the morphology-based enormous potential of polymer fibers for lightweight, cost-effective and recyclable full polymer solutions in compact components.

KEYWORDS

composites, manufacturing, mechanical properties, morphology, thermoplastics

1 | INTRODUCTION

Nowadays, additive manufacturing, also known as three-dimensional (3D) printing is increasingly utilized as a processing technique for the manufacturing of components made of different materials like metal or plastics. A printing process variant that is very suitable for plastics is so-called fused filament fabrication (FFF) or also known as fused deposition moldeling. Compared with traditional techniques for polymer processing, FFF exhibits great advantages in flexible and moldless manufacturing of customized components with complex shapes, which is also highlighted with a low material waste rate. With the development of the FFF technique, a lot of commercially available polymeric materials, such as polylactic acid,[1,2] acrynitrile butadiene styrene,[3,4] polypropylene (PP),[5–7] polycarbonate,[8,9] polyethylene terephthalate glycol-modified,[10] polyamide,[11] and so forth, have been already successfully applied.

FFF is based on the melting of a thermoplastic filament in a hot nozzle, which directionally deposits polymer strands according to precisely pre-defined paths layer-by-layer. Similar to conventional extrusion welding technology, completely melted polymer strands are

Dedicated to Professor Stoyko Fakirov on the occasion of his 85th birthday.

placed against previously deposited and now cooled strands and welded to them. The generation of the component from individual polymer strands ultimately leads to anisotropy in the properties. This peculiarity can be used positively in a targeted manner.

It is known from fiber-reinforced plastics that their ability to bear loads is greatest when the reinforcing fibers are aligned in the direction of the loads acting.

Therefore, in the recent past there has been intensive research into how the strategy of aligning fibers can improve the mechanical properties of printed components.[12–16] Ultimately, the investigations confirmed that glass or carbon fibers can be aligned well along the printing direction or raster direction, which leads to an improvement in the mechanical properties.[17–19] To date, however, there have been no studies on this with plastic fiber-reinforced plastics. In such materials, stretched plastics are combined with a coherent matrix. These materials essentially combine a low density with the morphologically high mechanical properties of polymers in fiber form. A special form of these materials, so-called microfibrillar composites MFC, was presented by Evstatiev and Fakirov three decades ago.[20] MFC are produced by a three-step-process as shown in Figure 1:

- Mixing: Compounding of two polymers and extrusion into a continuous filament.
- Fibrillation: Stretching the filament (cold or warm) to create highly oriented microfibrils.
- Post-processing: Processing at a temperature between the melting temperatures of the two polymers to ensure the formation of an isotropic matrix of the lower melting polymer, whereas the higher melting polymer still retaining the stretched highly oriented fibrils.

A few years ago, there was also intensive research into how this material can be improved by adding nanoparticles.[21–24] Although this is basically possible, it was found that during the production of parts by injection molding, the fiber orientation can hardly be controlled and the fibers are shortened, resulting hardly in a reinforcement effect of the fibers.[25,26]

In the present study, microfibrillar reinforced composite based on PP/poly(ethyleneterephthalate) (PET) blend in a 80/20 weight ratio were prepared by extrusion followed by cold drawing, and then printed using the FFF technique. Afterwards, morphological properties and tensile properties were characterized.

2 | MATERIALS AND METHODS

Commercial PP (HD 120MO, Borealis GmbH, Burghausen, Germany) and PET (Lighter C93, Equipolymers GmbH, Schkopau, Germany) were used as polymeric matrix and reinforcing component in this study, respectively. Compounding of the PP/PET blend was carried out on a co-rotated twin-screw extruder (ZSE 18 MAXX, Leistritz, Nürnberg, Germany). The barrel temperatures were set as 120/170/220/245/265/265/265/265/265/265/265°C in the 11 individual heating zones from the hopper to the die. The screw speed was 120 rpm. The PET content of the compound was 20% by weight.

The extruded strand was granulated, fed to a single-screw extruder (EX6, Filabot, Barre, USA) and a printable filament with a diameter of 1.8 ± 0.1 mm was produced in the process. The temperature at the barrel of the filament extruder were selected as 50/215/260/250°C from the hopper to the die. The screw speed was set at 5 rpm.

To create the microfibrillated structure, part of the extruded strand was drawn with a self-made filament stretching device in a warm water bath at 85°C. The drawn filament with a diameter of 0.7 ± 0.05 mm was granulated again and a printable filament with a diameter of 1.8 ± 0.1 mm was fabricated using again the single-screw filament extruder at a barrel temperatures 50/150/195/210°C from the hopper to the die.

3D printing of the specimens was performed on a modified FFF 3D printer (Ultimaker 2, Ultimaker B.V., Utrecht, Netherlands). All tensile testing specimens are printed along the longitudinal direction (0°) according to the international standard DIN ISO EN 527/1BB. The whole processing chain is shown in Figure 2.

Based on preliminary work we choose the FFF parameters as shown in Table 1. To overcome the warpage during printing, the first layer specimens was printed with a brim on a PP tape (tesa 64,014). The platform temperature was set at 140°C.

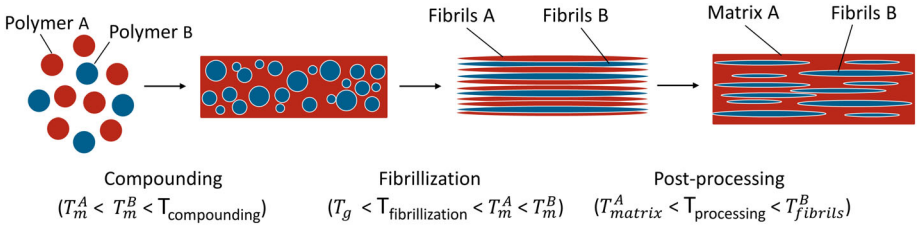

FIGURE 1 Basic procedure of microfibrillar composite (MFC) preparation [Color figure can be viewed at wileyonlinelibrary.com]

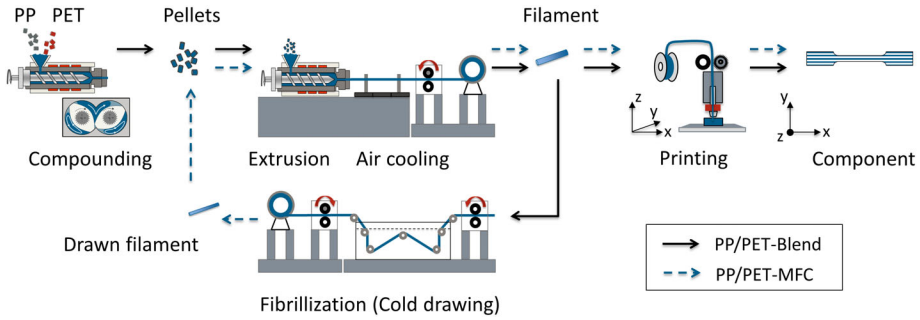

FIGURE 2 Schematic illustration of the whole processing chain [Color figure can be viewed at wileyonlinelibrary.com]

TABLE 1 3D printing parameters

Nozzle temperature	Platform temperature	Printing speed	Layer thickness	Orientation	Infill
°C	°C	mm/s	mm	°	%
210, 260[a]	140	5	0.2	0	100

Abbreviations: 3D, three-dimensional; PET, poly(ethylene terephthalate).
[a]Nozzle temperature was set at 260°C for printing neat PET.

The fracture surfaces of the extrudates, stretched filaments and 3D printed specimens were inspected using a Keyence confocal 3D laser scanning microscope (LSM, VK-X1050, Keyence Corporation, Japan). For better observation of fibrils, PET/PP stretched strands and MFC specimens were etched by xylene at 130°C for 1–3 h to remove the PP fraction.

The thermal properties of the polymers and composites were analyzed by a differential scanning calorimetry (DSC Q20, TA Instruments, USA). The thermal investigations were performed from 40 to 265°C with a heating/cooling rate of 10 K/min. The degree of crystallinity α_c for the PP phase was determined by using the following equation:

$$\alpha_c = \frac{\Delta H_m}{\Delta H_m^{\circ} w_f} \times 100\%, \quad (1)$$

is the theoretical specific enthalpy of completely crystallized PP (207 J/g). w_f represents the weight fraction of PP in the compound.

Tensile tests of the samples were conducted on a universal tensile testing machine according to the international standard DIN ISO EN 527/1BB. The crosshead speed was set at 1 and 50 mm/min for determining the tensile modulus and tensile strength, respectively. All the data presented correspond to the average of at least five measurements.

3 | RESULTS AND DISCUSSION

Figure 3(a) shows a typical incompatible sea-island morphology of the PP/PET blend after extrusion, in which the clear PET spherical domains are rather homogeneous and isotropic distributed in the PP matrix. The spherical droplet presents a wide distribution of a diameter from 3 to 17 μm with a mean value of around 9.6 μm. The drawn strand (Figure 3(b)), on the other hand, does not show a coherent PP matrix, but only thin filaments with a diameter range of 0.5–10 μm, that is, both PP and PET are in fiber form. In order to better determine the dimensions of the reinforcing PET fibers, the PP components were selectively removed by etching. Figure 3(c),(d) impressively shows that the PET fibers again consist of smaller fibrils with a diameter range of 0.5–1.2 μm. It is worthy of noting that the PET fibrils are quite long with the measured length up to 1500 μm. This high aspect ratios (length/diameter ratio) can be attributed to the two factors: the big size of the original PET droplets and a coalescence effect of the contacting elongated PET droplets.[25,27]

The 3D LSM images of the fracture surfaces of PET/PP 3D printed MFC are shown in Figure 4. First of all, it is noticeable that the fractured surface reveals fibrous bristles (indicated by the white arrow in Figure 4 (a)) in a diameter range of 5–10 μm. These bristles are homogeneously distributed in the composite and aligned almost unidirectionally in the direction of printing (Figure 4(a)). A scan of the topography of the fibers shows undulations with an apparent diameter of about 0.8 μm. When the polypropylene is selectively removed from the composite by chemical etching, smaller but still partially stuck together fibrils appear. After manual manipulation of this pile of fibers, individual microfibrils with a diameter of 0.5–1.2 μm become visible (Figure 4(c)).

The fracture mechanisms were characterized by inspecting the tensile fractured surfaces of the 3D printed

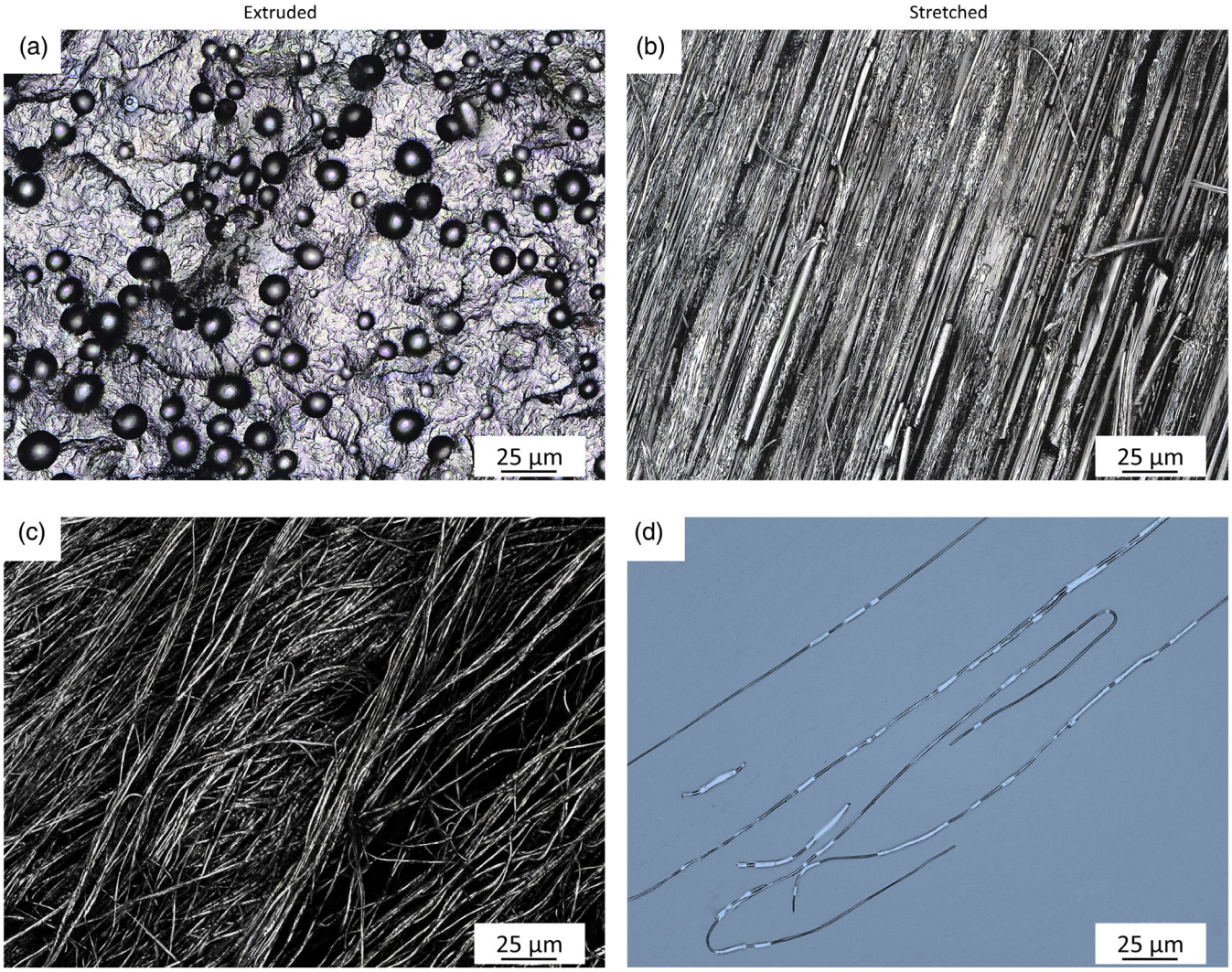

FIGURE 3 3D laser scanning microscope images: The cyro-fracture surfaces of (a) polypropylene/poly(ethylene terephthalate) (PP80/PET20) extruded blend and (b) stretched blend; (c) and (d) PET fibers in the stretched blend after extraction of the PP matrix [Color figure can be viewed at wileyonlinelibrary.com]

specimens (Figure 5). As is seen, the bonding between different sequential layers is excellent as no weld lines are visible, which is believed to be important for the mechanical properties of the printed components. The print raster or the individual print layers (layer height 0.2 mm) cannot be identified by inspecting the fracture surface (see Figure 5(a)) and cryo-fracture (Figure 5(d)) with the LSM. Decent bonding between the layers can therefore be assumed. A close view of the fractured surface clearly demonstrates that under the tensile strength some fibrils and fibril bundles were pulled out from the matrix, left cavities, which indicates poor bonding strength between the PET fibers and the PP matrix (Figure 5(c)). Nevertheless, some fiber bundles carry the load more effectively at tensile loading, which is indicated by fiber breakage (denoted by the white arrows in Figure 5(c)).

The DSC measurements were performed on the extruded PP/PET blend (PP/PET-extruded), their intermediate stretched PP/PET filament (PP/PET-stretched), final 3D printed PP/PET blend (PP/PET-3D-Blend), PP/PET microfibrillar composite (PP/PET-3D-MFC), neat PP (PP-3D) and PET (PET-3D) as well. The first heating curves and the first cooling curves are shown in Figure 6 and the relevant results are listed in Table 2. It can be seen that the extruded blend exhibits two melting temperatures T_m^{PP} and T_m^{PET}, at around 166 and 251°C and two crystallization temperatures T_c^{PP} and T_c^{PET} at around 122 and 206°C, respectively. After stretching, the melting temperature T_m^{PP} and percentage of crystallinity (X_m^{PP}) of the PP increases by 5.6°C and 8.5%, respectively. This phenomenon is presumably due to a strain-induced crystallization of the PP fibers. During drawing, the PP molecule chains are aligned along the stretching direction and

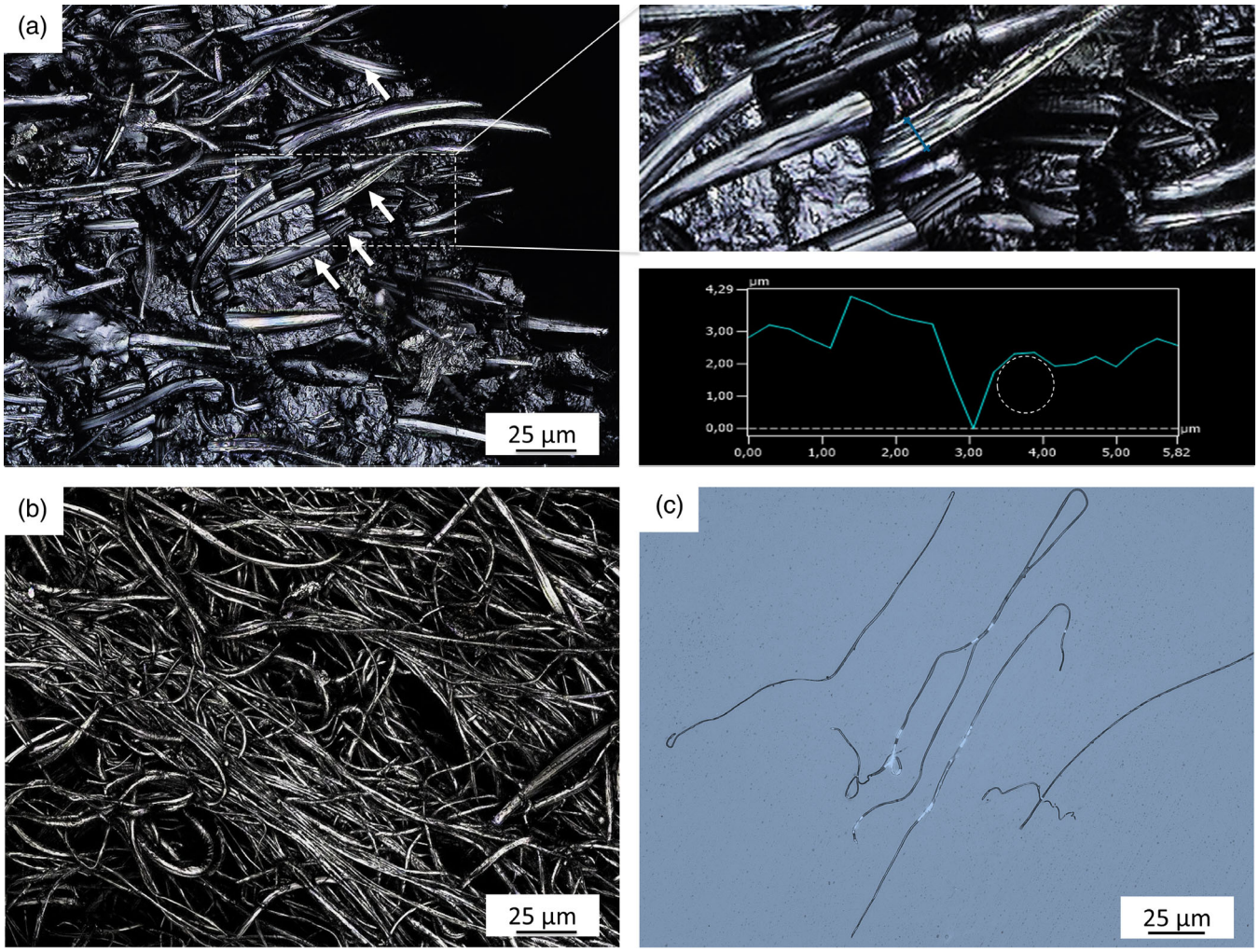

FIGURE 4 3D laser scanning micrographs: (a) the cyro-fracture surfaces of 3D printed microfibrillar composite (MFC) with height profile of fibers; and (b) and (c) poly(ethylene terephthalate) (PET) fibers in 3D printed MFC after extraction of the polyropylene (PP) matrix [Color figure can be viewed at wileyonlinelibrary.com]

then crystallize in a more perfect arrangement. The 3D-printed PP/PET blend and the PP/PET-MFC also show a higher T_c^{PP} and X_m^{PP} than PP, which suggests that PET also presumably supports crystallization through nucleation of the coherent PP matrix.[28,29] It is also well worth pointing out that the crystallinity of 3D printed PP/PET MFC is slightly higher than printed PP/PET blend, which indicates that PET microfibers exhibit a more pronounced nucleating effect on the crystallization of the PP matrix due to the higher surface-to-volume ratio.[30] Similar results on the injection-molded samples[25] and compression-molded samples[31] are also reported in the literature.

Figure 7 shows the mechanical properties of uniaxial, static tensile tests of printed specimens of the PP/PET blend and the PP/PET MFC in comparison with the characteristic values of the printed pure PP and PET (tested in the x-direction). It is immediately noticeable that the PET phase causes the reduction of the tensile strength of the blends compared to neat PP. In contrast, obvious improvement of the tensile strength and Young's modulus of the MFC can be observed, which increased by around 40% and 50% compared to the non-fibrillated form, respectively (Figure 7(b)). Compared with the pure PP, the measured strength and modulus of the MFC are around 15% and 66% higher, respectively. It is worth noting that with reinforcement of 20 wt% PET fibrils the MFC exhibits quite a high tensile modulus, which is comparable to the value of bulk PET. However, the tensile strength of MFC is much lower in contrast to those of PET. This can be attributed to the relatively poor fiber/matrix-interface, as shown in Figure 5(c) beforehand. Due to the weak fiber/matrix adhesion the forces cannot be transferred via shear to the fibers. Consequently the load carrying potential of the fibers cannot be fully exploited. All the above is attributed to a less pronounced

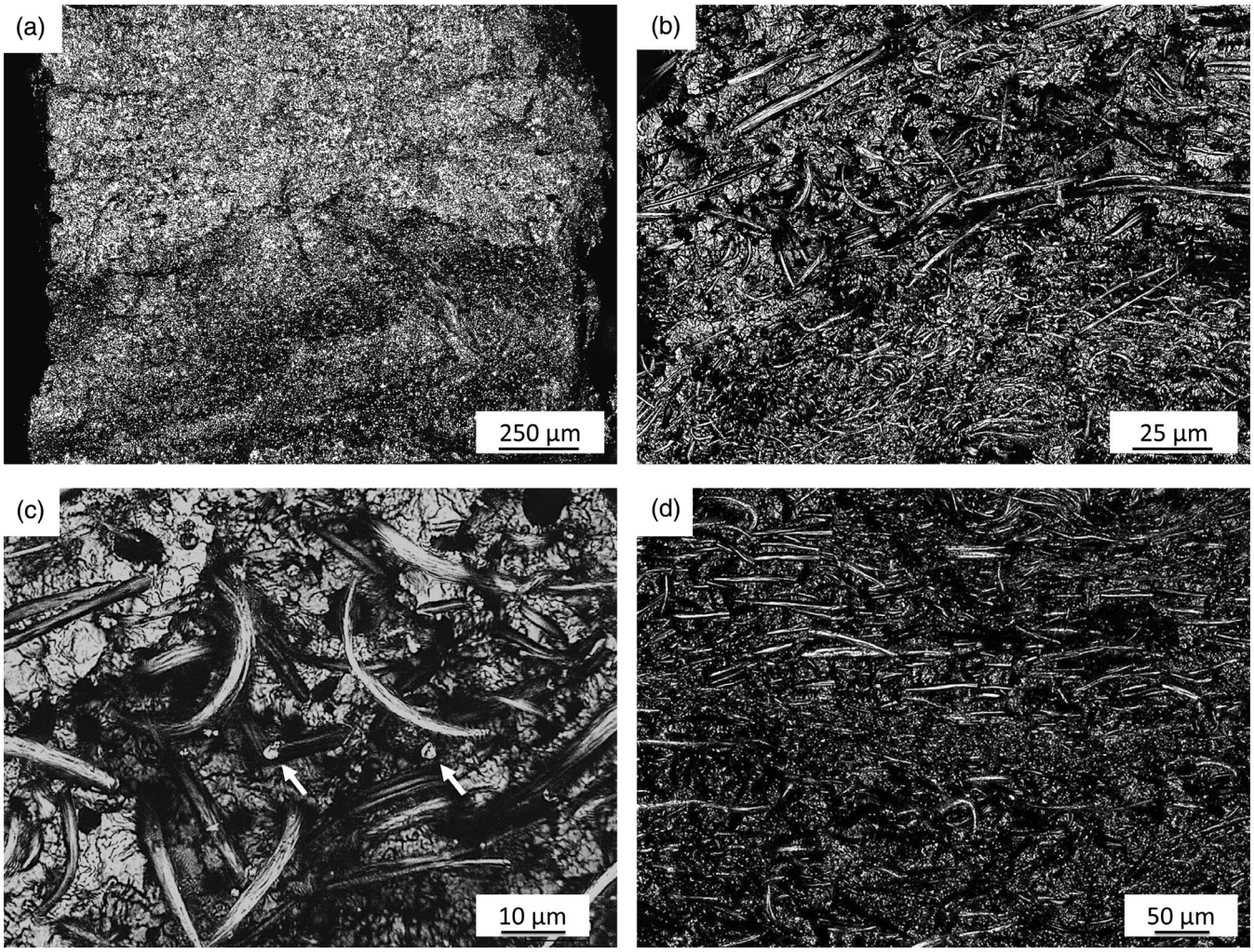

FIGURE 5 3D laser scanning micrographs of (a)–(c) the tensile fracture surfaces in yz-plane and (d) the cyro-fracture surfaces in xz-plane of 3D printed microfibrillar composite (MFC)

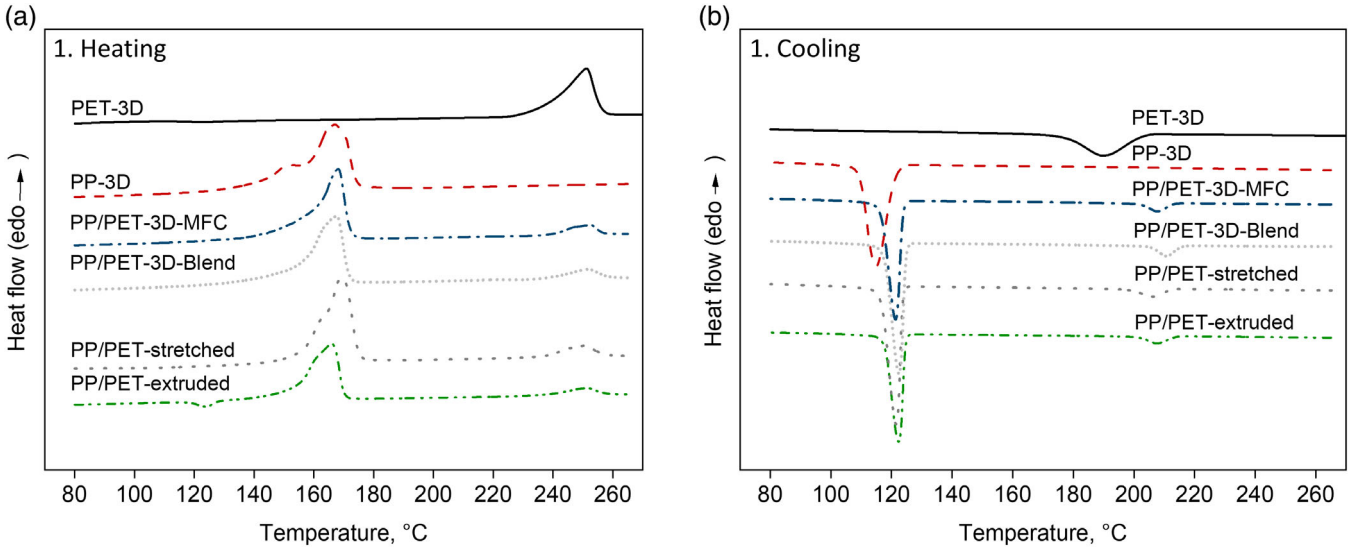

FIGURE 6 Differential scanning calorimetry (DSC) 1. Heating curves (a) and 1. Cooling curves (b) [Color figure can be viewed at wileyonlinelibrary.com]

TABLE 2 Thermal properties during 1. Heating and 1. Cooling

	1. Heating				1. Cooling			
Designation	T_m^{PP}, °C	ΔH_m^{PP}, J/g	T_m^{PET}, °C	ΔH_m^{PET}, J/g	X_m^{PP}, %	T_c^{PP}, °C	ΔH_c^{PP}, J/g	T_c^{PET}, °C
PET-3D	—	—	251.5	43.1	—	—	—	188.2
PP-3D	166.9	101.4	—	—	49.0	114.9	102.8	—
PP/PET-3D-MFC	166.8	86.7	252.0	9.6	52.4	121.4	82.3	207.8
PP/PET-3D-Blend	166.5	83.5	251.9	8.3	50.4	122.3	82.8	209.1
PP/PET-stretched	171.5	83.1	250.0	9.7	50.2	120.9	82.3	213.3
PP/PET-extruded	165.9	69.1	251.4	8.9	41.7	122.1	82.1	205.7

Abbreviations: 3D, three-dimensional; MFC, microfibrillar composite; PET, poly(ethylene terephthalate); PP, polypropylene.

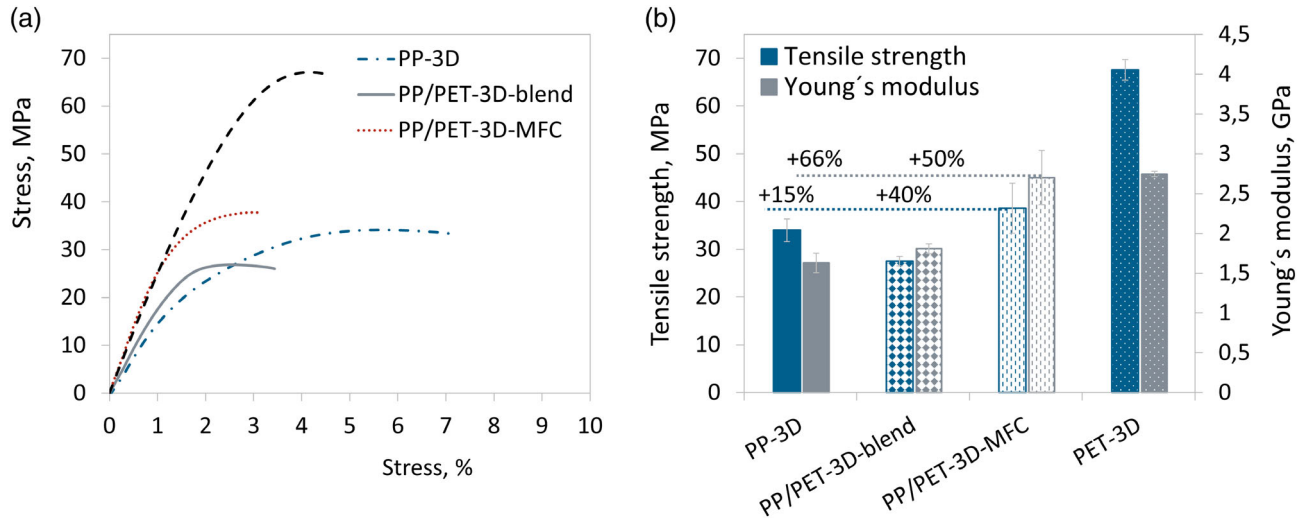

FIGURE 7 Tensile properties of 3D printed samples: (a) representative stress–strain curve, (b) tensile strength and Young's modulus [Color figure can be viewed at wileyonlinelibrary.com]

enhancement of tensile strength. In parallel, the MFC presents a significantly lower elongation at break compared with pure materials (Figure 7(a)).

4 | CONCLUSIONS

In this study, an MFC composite was successfully produced by melt extrusion and cold stretching. The LSM images show that the highly oriented PET fibrils of the extruded filament were excellently preserved in the 3D printed parts made from them along the printing direction.

The results demonstrate the feasibility of combining 3D printing with microfibrillar reinforced composite materials for the flexible design and manufacture of highly material-efficient and recyclable full polymer components.

The DSC analysis shows that the crystallization temperatures of the PP phase were shifted to higher temperatures in both the PP/PET blend and in the MFC, which indicates that PET acts as a nucleating agent. In addition, a higher degree of crystallinity is observed in the MFC compared to both printed pure PP and a PP/PET blend, which shows that the PET fibrils allow more perfect crystallization of the PP matrix.

PP/PET MFC displays obvious improvement of mechanical properties compared to neat PP and a PP/PET blend, due to the reinforcing effect of the PET fibrils. A further improvement in mechanical performance is likely to be achieved by improving the filamentation of the PET down to the single fiber diameter, optimizing the adhesion between the PET fibrils and the PP matrix by using a compatibilizer, adjusting the viscosity ratio between PP and PET, and increasing the PET-content in the composite.

ACKNOWLEDGMENTS

The authors are grateful to Borealis GmbH, Burghausen, and Equipolymers GmbH, Schkopau, for the supply of the materials. TECHNISCHE UNIVERSITAET KAISERSLAUTERN Blended DEAL: Projekt DEAL.

ORCID

Alois K. Schlarb https://orcid.org/0000-0001-8693-9163

REFERENCES

[1] J. M. Reverte, M. A. Caminero, J. M. Chacón, E. García-Plaza, P. J. Núñez, J. P. Becar, *Materials* **2020**, *13*, 1924.

[2] R. Hashemi Sanatgar, C. Campagne, V. Nierstrasz, *Appl. Surf. Sci.* **2017**, *403*, 551.

[3] S. Rohde, J. Cantrell, A. Jerez, C. Kroese, D. Damiani, R. Gurnani, L. DiSandro, J. Anton, A. Young, D. Steinbach, P. Ifju, *Exp. Mech.* **2018**, *58*, 871.

[4] K. Raney, E. Lani, D. K. Kalla, *Mater. Today Proc.* **2017**, *4*, 7956.

[5] O. S. Carneiro, A. F. Silva, R. Gomes, *Mater. Des.* **2015**, *83*, 768.

[6] L. Wang, D. J. Gardner, *Polymer* **2017**, *113*, 74.

[7] Y. G. Zhou, B. Su, L. S. Turng, *Rapid Prototyp. J.* **2017**, *23*, 869.

[8] M. J. Reich, A. L. Woern, N. G. Tanikella, J. M. Pearce, *Materials* **2019**, *12*, 1642.

[9] A. Reyes-Rodríguez, R. Dorado-Vicente, R. Mayor-Vicario, *Proc. Manuf.* **2017**, *13*, 880.

[10] K. Durgashyam, M. Indra Reddy, A. Balakrishna, K. Satyanarayana, *Mater. Today Proc.* **2019**, *18*, 2052.

[11] Y. Zhang, C. Purssell, K. Mao, S. Leigh, *Tribol. Int.* **2020**, *141*, 105953.

[12] G. Liao, Z. Li, Y. Cheng, D. Xu, D. Zhu, S. Jiang, J. Guo, X. Chen, G. Xu, Y. Zhu, *Mater. Des.* **2018**, *139*, 283.

[13] X. Tian, T. Liu, C. Yang, Q. Wang, D. Li, *Composites, Part A* **2016**, *88*, 198.

[14] W. Zhong, F. Li, Z. Zhang, L. Song, Z. Li, *Mater. Sci. Eng., A* **2001**, *301*, 125.

[15] G. Sodeifian, S. Ghaseminejad, A. A. Yousefi, *Results Phys.* **2019**, *12*, 205.

[16] Stepashkin, D. I. Chukov, F. S. Senatov, A. I. Salimon, A. M. Korsunsky, S. D. Kaloshkin, *Compos. Sci. Technol.* **2018**, *164*, 319.

[17] P. Parandoush, D. Lin, *Compos. Struct.* **2017**, *182*, 36.

[18] Hofstätter, T.; Gutmann, I. W.; Koch, T.; Pedersen, D. B.; Tosello, G.; Heinz, G.; Hansen, H. N. In Proceedings - ASPE/euspen 2016 Summer Topical Meeting: Dimensional Accuracy and Surface Finish in Additive Manufacturing, Raleigh, USA, June 27–30, **2016**.

[19] H. L. Tekinalp, V. Kunc, G. M. Velez-Garcia, C. E. Duty, L. J. Love, A. K. Naskar, C. A. Blue, S. Ozcan, *Compos. Sci. Technol.* **2014**, *105*, 144.

[20] M. Evstatiev, S. Fakirov, *Polymer* **1992**, *33*, 877.

[21] W. Li, A. K. Schlarb, M. Evstatiev, *J. Polym. Sci. Part B Polym. Phys.* **2009**, *47*, 555.

[22] W. Li, A. K. Schlarb, M. Evstatiev, *J. Appl. Polym. Sci.* **2009**, *113*, 1471.

[23] W. Li, A. K. Schlarb, M. Evstatiev, *J. Appl. Polym. Sci.* **2009**, *113*, 3300.

[24] W. Li, J. Karger-Kocsis, A. K. Schlarb, *Macromol. Mater. Eng.* **2009**, *294*, 582.

[25] M. Kuzmanović, L. Delva, L. Cardon, K. Ragaert, *Polymers* **2016**, *8*, 355.

[26] K. Jayanarayanan, S. Thomas, K. Joseph, *Composites, Part A* **2008**, *39*, 164.

[27] S. Fakirov, *Synthetic Polymer-Polymer Composites*, (Eds: D. Bhattacharyya, S. Fakirov) Carl Hanser Verlag, Munich, Germany **2012**, p. 351. https://doi.org/10.3139/9781569905258

[28] Y. Zhu, C. Liang, Y. Bo, S. Xu, *J. Polym. Res.* **2015**, *22*, 35.

[29] F. Mirjalili, S. Moradian, F. Ameri, *Sci. World J.* **2013**, *13*, 468542.

[30] Y. Zhu, C. Liang, Y. Bo, S. Xu, *J. Therm. Anal. Calorim.* **2015**, *119*, 2005.

[31] Y. C. Dong, J. P. Xu, S. Fan, *Plast. Rubber Compos.* **2017**, *46*, 1.

How to cite this article: Huang M, Schlarb AK. Polypropylene/poly(ethylene terephthalate) microfibrillar reinforced composites manufactured by fused filament fabrication. *J Appl Polym Sci*. 2021;138:e50557. https://doi.org/10.1002/app.50557